Cross-scale interaction of host tree size and climate governs bark beetle-induced tree mortality

Abstract word count: 348

Overall .docx word count: 12959

Main text word count: 4684 (Intro: 1536; Results: 456 (45+119+292); Discussion: 2692)

Methods word count: 2903 (697+642+1564)

Text boxes word count: 0

Date report generated: May 04, 2020

Abstract

The Californian hot drought of 2012 to 2015 created favorable conditions for unprecedented ponderosa pine (*Pinus ponderosa*) mortality in the Sierra Nevada mountain range, largely attributable to the western pine beetle (*Dendroctonus brevicomis*; WPB). Climate conditions can partially explain tree mortality patterns through their direct effect on tree vigor, but tree mortality rates can respond non-linearly to climate conditions when bark beetles interact with local forest characteristics while they colonize drought-stressed trees. Measuring broad-scale climate conditions simultaneously with local forest composition and structure– the spatial distribution and size of trees– will refine our understanding of how these variables interact, but is generally expensive and/or labor-intensive. We use drone surveys over 32 distinct sites along a 350-km latitudinal and 1000-m elevational gradient in western slope Sierra Nevada ponderosa pine/mixed-conifer forests and structure from motion (SfM) photogrammetry to segment and classify more than 450,000 trees over 9 km^2 of forest with WPB-induced tree mortality. We validated the segmentation and classification with data from 160 coincident field plots (each 0.041 ha in area) throughout the 32 sites, assuming that dead trees were all ponderosa pine killed by WPB. We modeled the probability of ponderosa pine mortality as a function of forest structure and composition and their interaction with site-level climatic water deficit (CWD), accounting for spatial covariance using exact Gaussian processes. A greater local proportion of host trees strongly increased the probability of host mortality, with greater host density amplifying this effect. Further, we found a strong interaction between host size and CWD such that larger trees increased the probability of host mortality at hot/dry sites, but smaller trees tended to drive mortality in cool/wet sites. Our results demonstrate a variable response of WPB to local forest structure and composition across an environmental

1

gradient, which may help reconcile differences between observed ecosystem-wide tree mortality patterns and predictions from models based on coarser-scale forest structure. Climate change adaptation strategies should consider that future disturbance outcomes may depend on interactions between local forest structure and broad-scale environmental gradients, with the potential for cross-scale interactions that challenge our current understanding of forest insect dynamics.

Introduction

Bark beetles dealt the final blow to many of the nearly 150 million trees killed in the California hot drought of 2012 to 2015 and its aftermath (USDAFS 2019). A harbinger of climate change effects to come, record high temperatures exacerbated the drought (Griffin and Anchukaitis 2014, Robeson 2015), which increased water stress in trees (Asner et al. 2016, Brodrick and Asner 2017), making them more susceptible to colonization by bark beetles (Fettig 2012, Kolb et al. 2016). Further, a century of fire suppression has enabled forests to grow into dense stands, which can also make them more vulnerable to bark beetles (Waring and Pitman 1985, Fettig 2012, Restaino et al. 2019). This combination of environmental conditions and forest structural characteristics led to tree mortality events of unprecedented size across the state (Young et al. 2017, USDAFS 2017).

Tree mortality exhibited a strong latitudinal and elevational gradient (Asner et al. 2016, Young et al. 2017) that can only be partially explained by coarse-scale measures of environmental conditions (i.e., historic climatic water deficit; CWD) and current forest structure (i.e., current regional basal area) (Young et al. 2017). Progressive loss of canopy water content offers additional insight into tree vulnerability to mortality, but cannot ultimately resolve which trees die in forests with bark beetles as a key mortality agent (Brodrick and Asner 2017). Bark beetles respond to local forest characteristics in positive feedbacks that non-linearly alter tree mortality dynamics against a background of environmental conditions that stress trees (Raffa et al. 2008, Boone et al. 2011). Thus, an explicit consideration of local forest structure and composition (Stephenson et al. 2019, Fettig et al. 2019) as well as its cross-scale interaction with regional climate conditions (Senf et al. 2017) can refine our understanding of tree mortality patterns from California's recent hot drought. The challenge of simultaneously measuring the effects of both local-scale forest features (such as structure and composition) and broad-scale environmental conditions (such as climatic water deficit; CWD) on forest insect disturbance leaves their interaction effect relatively underexplored (Seidl et al. 2016, Senf et al. 2017, Stephenson et al. 2019, Fettig et al. 2019).

The ponderosa pine/mixed-conifer forests in California's Sierra Nevada region are characterized by regular bark beetle disturbances, primarily by the influence of western pine beetle (*Dendroctonus brevicomis*; WPB)

on its host ponderosa pine (*Pinus ponderosa*) (Fettig 2016). WPB is a primary bark beetle– its reproductive success is contingent upon host tree mortality, which itself requires enough beetles to mass attack the host tree and overwhelm its defenses (Raffa and Berryman 1983). This Allee effect creates a strong coupling between beetle selection behavior of host trees and host tree susceptibility to colonization (Raffa and Berryman 1983, Logan et al. 1998, Wallin and Raffa 2004). A key defense mechanism of conifers to bark beetle attack is to flood beetle bore holes with resin, which physically expels colonizing beetles, can be toxic to the colonizers and their fungi, and may interrupt beetle communication (Franceschi et al. 2005, Raffa et al. 2015). Under normal conditions, weakened trees with compromised defenses are the most susceptible to colonization and will be the main targets of primary bark beetles like WPB (Bentz et al. 2010, Boone et al. 2011, Raffa et al. 2015). Under severe water stress, many trees no longer have the resources available to mount a defense (Boone et al. 2011, Kolb et al. 2016) and thus prolonged drought can often trigger increased bark beetle-induced tree mortality as average tree vigor declines (Bentz et al. 2010) (though we note that the inciting factors for increased tree mortality in other bark beetle systems, such as mountain pine beetle (*D. ponderosae*) in lodgepole pine (*P. contorta*), may be more related to temperature's effect on the beetle's physiology). As the local population density of beetles increases due to successful reproduction within spatially-aggregated weakened trees, as might occur during drought, mass attacks grow in size and become capable of overwhelming formidable tree defenses such that even healthy trees may be susceptible to colonization and mortality (Bentz et al. 2010, Boone et al. 2011, Raffa et al. 2015). Thus, water stress can be a key determinant of whether individual trees are susceptible to bark beetles under many conditions, and this environmental condition may interact with beetle population dynamics to drive tree susceptibility under extreme conditions (Bentz et al. 2010, Boone et al. 2011, Stephenson et al. 2019).

WPB activity is strongly influenced by forest structure– the spatial distribution and size of trees– and tree species composition. Taking forest structure alone, high-density forests are more prone to bark beetle-induced tree mortality (Fettig 2012) which may arise as greater competition for water resources amongst crowded trees and thus average tree resistance is lower (Hayes et al. 2009), or because smaller gaps between trees protect pheromone plumes from dissipation by the wind and thus enhance intraspecific beetle communication (Thistle et al. 2004). Tree size is another aspect of forest structure that affects bark beetle host selection behavior with smaller trees tending to have lower capacity for resisting attack, and larger trees being more desirable targets on account of their thicker phloem providing greater nutritional content (Miller and Keen 1960, Chubaty et al. 2009, Boone et al. 2011, Graf et al. 2012). Throughout an outbreak, some bark beetle species will collectively "switch" the preferred size of tree to attack in order to navigate the trade-off between host susceptibility and host quality (Geiszler and Gara 1978, Klein et al. 1978, Mitchell and Preisler 1991, Preisler

3

1993, Wallin and Raffa 2004). Taking forest composition alone, WPB activity in the Sierra Nevada mountain range of California is necessarily tied to the regional distribution of its exclusive host, ponderosa pine (Fettig 2016). Colonization by primary bark beetles can also depend on the relative frequencies of tree species in a more local area, akin to reduced oligophagous insect herbivory in forests comprising taxonomically-distinct tree species compared to monocultures (Jactel and Brockerhoff 2007).

The interaction between forest structure and composition also drives WPB activity. For instance, dense forests with high host availability may experience greater beetle-induced tree mortality because dispersal distances between potential host trees are shorter reducing predation of adults searching for hosts and facilitating higher rates of colonization (Miller and Keen 1960, Berryman 1982, Fettig et al. 2007), or because high host availability reduces the chance of individual beetles wasting their limited resources flying to and landing on a non-host tree (Moeck et al. 1981, Evenden et al. 2014). Stand-scale measures of forest structure and composition thus paint a fundamentally limited picture of the mechanisms by which these forest characteristics affect bark beetle disturbance, but finer-grain information explicitly recognizing tree species, size, and local density should better capture the ecological processes underlying insect-induced tree mortality (Geiszler and Gara 1978, Mitchell and Preisler 1991, Preisler 1993, Kaiser et al. 2013). Additionally, considering the effects of local forest structure and composition with the effects of environmental conditions may help refine our understanding of tree mortality patterns in widespread events, such as during the recent California hot drought.

The vast spatial extent of tree mortality in the 2012 to 2015 California hot drought challenges our ability to simultaneously consider how broad-scale environmental conditions may interact with local forest structure and composition to affect the dynamic between bark beetle selection and colonization of host trees, and host tree susceptibility to attack (Anderegg et al. 2015, Stephenson et al. 2019). Measuring local forest structure generally requires expensive instrumentation (Kane et al. 2014, Asner et al. 2016) or labor-intensive field surveys (Larson and Churchill 2012, Stephenson et al. 2019, Fettig et al. 2019), which constrains survey extent and frequency. Small, unhumanned aerial systems (sUAS) enable relatively fast and cheap remote imaging over hundreds of hectares of forest, which can be used to measure complex forest structure and composition at the individual tree scale with Structure from Motion (SfM) photogrammetry (Morris et al. 2017, Shiklomanov et al. 2019). The ultra-high resolution of sUAS-derived measurements as well as the ability to incorporate vegetation reflectance can help overcome challenges in species classification and dead tree detection inherent in other remote sensing methods, such as airborne LiDAR (Jeronimo et al. 2019). Distributing such surveys across an environmental gradient can overcome the data acquisition challenge inherent in investigating phenomena with both a strong local- and a strong broad-scale component.

4

We used sUAS-derived remote sensing images over a network of 32 sites in Sierra Nevada ponderosa pine/mixed-conifer forests spanning 1000 m of elevation and 350 km of latitude (see Fettig et al. 2019) covering a total of 9 km^2, to investigate how broad-scale environmental conditions interacted with local forest structure and composition to shape patterns of tree mortality during the cumulative tree mortality event of 2012 to 2018. We asked:

1. How does the proportion of host trees in a local area and average host tree size affect WPB-induced tree mortality?

2. How does the density of all tree species (hereafter "overall density") affect WPB-induced tree mortality?

3. How does the total basal area of all tree species (hereafter "overall basal area") affect WPB-induced tree mortality?

4. How does environmentally-driven tree moisture stress affect WPB-induced tree mortality?

5. Do the effects of forest structure, forest composition, and environmental condition interact to influence WPB-induced tree mortality?

Methods

Study system

We built our study coincident with 160 vegetation/forest insect monitoring plots at 32 sites established between 2016 and 2017 by Fettig et al. (2019) (Figure 1). The study sites were chosen to reflect typical west-side Sierra Nevada yellow pine/mixed-conifer forests and were dominated by ponderosa pine (Fettig et al. 2019). Plots were located in WPB-attacked, yellow pine/mixed-conifer forests across the Eldorado, Stanislaus, Sierra and Sequoia National Forests and were stratified by elevation (914-1219 m, 1219-1524 m, 1524-1829 m above sea level). In the Sequoia National Forest, the southernmost National Forest in our study, plots were stratified with the lowest elevation band of 1219-1524 m and extended to an upper elevation band of 1829-2134 m to capture a more similar forest community composition as at the more northern National Forests. The sites have variable forest structure and plot locations were selected in areas with >35% ponderosa pine basal area and >10% ponderosa pine mortality. At each site, five 0.041-ha circular plots were installed along transects with 80 to 200m between plots. In the field, Fettig et al. (2019) mapped all stem locations relative to the center of each plot using azimuth/distance measurements. Tree identity to species, tree height, and diameter at breast height (DBH) were recorded if DBH was greater than 6.35cm. Year of mortality was estimated based on needle color and retention if it occurred prior to plot establishment, and was directly observed thereafter during annual site visits. A small section of bark (approximately 625
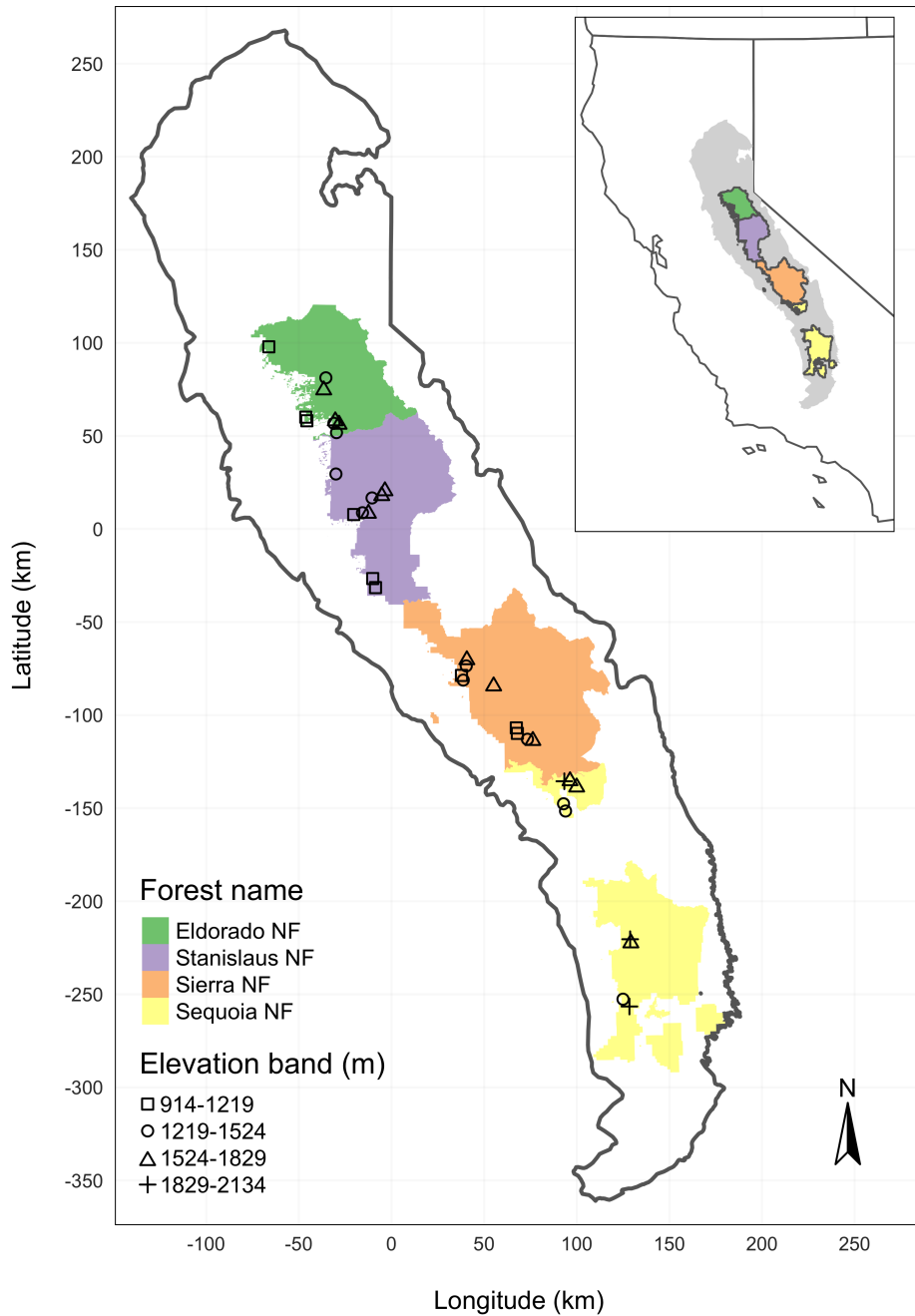
Figure 1: The network of field plots spanned a 350-km latitudinal gradient from the Eldorado National Forest in the north to the Sequoia National Forest in the south. Plots were stratified by three elevation bands in each forest, with the plots in the Sequoia National Forest (the southern-most National Forest) occupying elevation bands 305 m above the three bands in the other National Forests in order to capture a similar community composition.

cm^2) on both north and south aspects was removed from dead trees to determine if bark beetle galleries were present. The shape, distribution, and orientation of galleries are commonly used to distinguish among bark beetle species (Fettig 2016). In some cases, deceased bark beetles were present beneath the bark to supplement identifications based on gallery formation. During the spring and early summer of 2018, all field plots were revisited to assess whether dead trees had fallen (Fettig et al. 2019).

In the typical life cycle of WPBs, females initiate host colonization by tunneling through the outer bark and into the phloem and outer xylem where they rupture resin canals.

As a result, oleoresin exudes and collects on the bark surface, as is commonly observed with other bark beetle species. During the early stages of attack, females release an aggregation pheromone component which, in combination with host monoterpenes released from pitch tubes, is attractive to conspecifics (Bedard et al. 1969). An antiaggregation pheromone component is produced during latter stages of host colonization by several pathways, and is thought to reduce intraspecific competition by altering adult behavior to minimize overcrowding of developing brood within the host (Byers and Wood 1980). Volatiles from several nonhosts sympatric with ponderosa pine have been demonstrated to inhibit attraction of WPB to its aggregation pheromones (Fettig et al. 2005, Shepherd et al. 2007). In California, WPB generally has 2-3 generations in a single year and can often out-compete other primary bark beetles such as the mountain pine beetle in ponderosa pines, especially in larger trees (Miller and Keen 1960).

Aerial data collection and processing

Nadir-facing imagery was captured using a gimbal-stabilized DJI Zenmuse X3 broad-band red/green/blue (RGB) camera (DJI 2015a) and a fixed-mounted Micasense Rededge3 multispectral camera with five narrow bands (Micasense 2015) on a DJI Matrice 100 aircraft (DJI 2015b). Imagery was captured from both cameras along preprogrammed aerial transects over ~40 ha surrounding each of the 32 sites (each of these containing five field plots) and was processed in a series of steps to yield local forest structure and composition data suitable for our statistical analyses. All images were captured in 2018 during a 3-month period between early April and early July, and thus our work represents a postmortem investigation into the drivers of cumulative tree mortality. Following the call by Wyngaard et al. (2019), we establish "data product levels" to reflect the image processing pipeline from raw imagery (Level 0) to calibrated, fine-scale forest structure and composition information on regular grids (Level 4), with each new data level derived from levels below it. Here, we outline the steps in the processing and calibration pipeline visualized in Figure 2, and include additional details in the Supplemental Information.
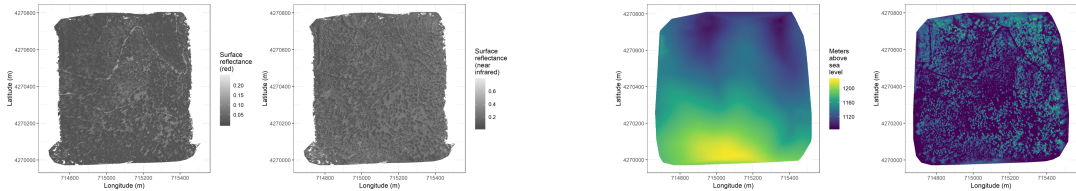
7

Level 0: raw data from sensors
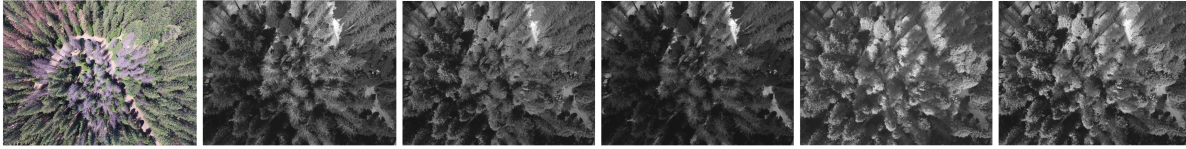
Level 1: basic outputs from photogrammetric processing

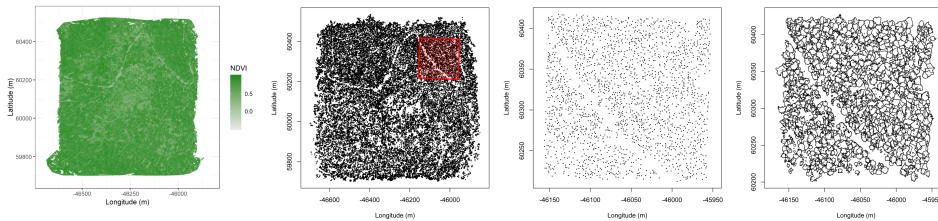# Level 2: corrected outputs from photogrammetric processing

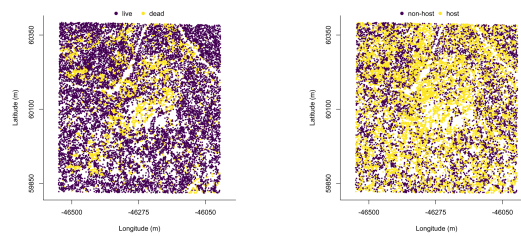radiometric (e.g., normalize for atmosphere)   geometric (e.g., normalize for terrain)
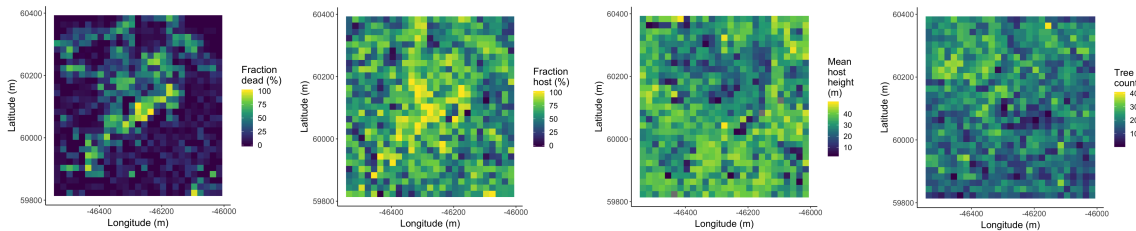
Level 3: domain-specific information extraction

L3a
spectral
OR
geometric

L3b
spectral
AND
geometric

Level 4: aggregations to regular grids

Figure 2. Schematic of the data processing workflow for a single site with each new data product level derived from data at lower levels.

Level 0 represents raw data from the sensors. From left to right: example broad-band RGB photo from DJI Zenmuse X3 camera, example blue photo from Rededge3 (centered on 475nm), example green photo from Rededge3 (centered on 560nm), example red photo from Rededge3 (centered on 668nm), example near infrared photo from Rededge3 (centered on 840nm), and example red edge photo from Rededge3 (centered on 717nm).

Level 1 represents basic outputs from the photogrammetric workflow, in this case implemented with Pix4Dmapper. From left to right: a dense point cloud visualized in CloudCompare (https://www.danielgm.net/cc/), an orthophoto generated from the RGB camera, and a digital surface model representing the altitude above sea level (ground height + vegetation height) for every cell.

Level 2 represents outputs from photogrammetric processing that have been corrected radiometrically or geometrically. From left to right: a radiometrically-corrected surface reflectance map of the red narrow band from the Rededge3 camera, a radiometrically-corrected surface reflectance map of the near infrared narrow band from the Rededge3 camera, a rasterized version of the digital terrain model derived by a geometric correction of the dense point cloud, and a canopy height model derived by subtracting the terrain height from the digital surface model.

Level 3 represents domain-specific information extraction from Level 2 products and is divided into two sub-levels. Level 3a products are derived using only spectral or only geometric data. From left to right: a reflectance map of Normalized Difference Vegetation Index (NDVI; Rouse et al. 1973) derived using the red and near infrared Level 2 reflectance products, a map of points representing detected trees from the canopy height model with a red polygon highlighting the area presented in more detail for the next two images, a close-up of points representing detected trees, and a close-up of polygons representing segmented tree crowns. Level 3b products are derived using both spectral and geometric data. From left to right: a map of the point locations of detected trees that have been classified as alive or dead based on the pixel values within each segmented tree crown and a map of the point locations of detected trees classified to WPB host/non-host using the same spectral information. Note that our study relies on the generation of Level 3a products in order to combine them and create Level 3b products, but this need not be the case. For instance, deep learning/neural net methods may be able to use both the spectral and geometric information from Level 2 simultaneously to locate and classify trees in a scene and directly generate Level 3b products without a need to first generate the Level 3a products shown in this schematic (Weinstein et al. 2019, dos Santos et al. 2019).

Level 4 represents aggregations of Level 3 products to regular grids which might better reflect the grain size of the data for which we have the best calibration and thus the most confidence or which might provide new information not possible at an individual-tree level (e.g., average distance between trees in a small neighborhood). From left to right: aggregation of live/dead classified trees as fraction of dead trees in a 20 x 20-m cell, aggregation of host/non-host classified trees as fraction of hosts in a 20 x 20-m cell, aggregation of mean host height in a 20 x 20-m cell, and aggregation of tree count (including all species), in a 20 x 20-m cell. In our case, the 20 x 20-m aggregation produces a grid cell with an area of 400 m^2, which most closely matches the 404-m^2 area of the ground-based vegetation plots whose data we used in an aggregated form to calibrate our derivation of Level 3 products.

Level 0: Raw data from sensors

Raw data comprised approximately 1900 images per camera lens (one broad-band RGB lens and five narrow-band multispectral lenses) for each of the 32 sites (Figure 2; Level 0). Prior to the aerial survey, two strips of bright orange drop cloth (~100 x 15 cm) were positioned as an "X" over the permanent monuments marking the center of the 5 field plots from Fettig et al. (2019) (see Supplemental Information).

We preprogrammed north-south aerial transects using Map Pilot for DJI on iOS flight software (Drones-MadeEasy 2018) at an altitude of 120 m above ground level (with "ground" defined using a 1-arc-second digital elevation model (Farr et al. 2007)). The resulting ground sampling distance was approximately 5 cm/px for the Zenmuse X3 RGB camera and approximately 8 cm/px for the Rededge3 multispectral camera. We used 91.6% image overlap (both forward and side) at the ground for the Zenmuse X3 RGB camera and 83.9% overlap (forward and side) for the Rededge3 multispectral camera.

Level 1: Basic outputs from photogrammetric processing

We used SfM photogrammetry implemented in Pix4Dmapper Cloud (www.pix4d.com) to generate dense point clouds (Figure 2; Level 1, left), orthophotos (Figure 2; Level 1, center), and digital surface models (Figure 2; Level 1, right) for each field site (Frey et al. 2018). For 29 sites, we processed the Rededge3 multispectral imagery alone to generate these products. For three sites, we processed the RGB and the multispectral imagery together to enhance the point density of the dense point cloud. All SfM projects resulted in a single processing "block," indicating that all images in the project were optimized and processed together. The dense point cloud represents x, y, and z coordinates as well as the color of millions of points per site. The orthophoto represents a radiometrically uncalibrated, top-down view of the survey site that preserves the relative x-y positions of objects in the scene. The digital surface model is a rasterized version of the dense

point cloud that shows the altitude above sea level for each pixel in the scene at the ground sampling distance of the camera that generated the Level 0 data.

Level 2: Corrected outputs from photogrammetric processing

Radiometric corrections

A radiometrically-corrected reflectance map (Figure 2; Level 2, left two figures; i.e., a corrected version of the Level 1 orthophoto) was generated using the Pix4D software by incorporating incoming light conditions for each narrow band of the Rededge3 camera (captured simultaneously with the Rededge3 camera using an integrated downwelling light sensor) as well as a pre-flight image of a calibration panel of known reflectance (see Supplemental Information for camera and calibration panel details).

Geometric corrections

We implemented a geometric correction to the Level 1 dense point cloud and digital surface model by normalizing these data for the terrain underneath the vegetation. We generated the digital terrain model representing the ground underneath the vegetation at 1-m resolution (Figure 2; Level 2, third image) by classifying each survey area's dense point cloud into "ground" and "non-ground" points using a cloth simulation filter algorithm (Zhang et al. 2016) implemented in the `lidR` (Roussel et al. 2019) package and rasterizing the ground points using the `raster` package (Hijmans et al. 2019). We generated a canopy height model (Figure 2; Level 2, fourth image) by subtracting the digital terrain model from the digital surface model.

Level 3: Domain-specific information extraction

Level 3a: Data derived from spectral OR geometric Level 2 product

Using just the spectral information from the radiometrically-corrected reflectance maps, we calculated several vegetation indices including the normalized difference vegetation index (NDVI; Rouse et al. (1973); Figure 2; Level 3a, first image), the normalized difference red edge (NDRE; Gitelson and Merzlyak (1994)), the red-green index (RGI; Coops et al. (2006)), the red edge chlorophyll index ($CI_{red\ edge}$; Clevers and Gitelson (2013)), and the green chlorophyll index (CI_{green}; Clevers and Gitelson (2013)).

Table 1: Algorithm name, number of parameter sets tested for each algorithm, and references.

Algorithm	Parameter sets tested	Reference(s)
li2012	131	Li et al. (2012); Jakubowski et al. (2013); Shin et al. (2018)

11

Algorithm	Parameter sets tested	Reference(s)
lmfx	30	Roussel (2019)
localMaxima	6	Roussel et al. (2019)
multichm	1	Eysn et al. (2015)
ptrees	3	Vega et al. (2014)
vwf	3	Plowright (2018)
watershed	3	Pau et al. (2010)

Using just the geometric information from the canopy height model or terrain-normalized dense point cloud, we generated maps of detected trees (Figure 2; Level 3a, second and third images) by testing a total of 7 automatic tree detection algorithms and a total of 177 parameter sets (Table 1). We used the field plot data to assess each tree detection algorithm/parameter set by converting the distance-from-center and azimuth measurements of the trees in the field plots to x-y positions relative to the field plot centers distinguishable in the Level 2 reflectance maps as the orange fabric X's that we laid out prior to each flight. In the reflectance maps, we located 110 out of 160 field plot centers while some plot centers were obscured due to dense interlocking tree crowns or because a plot center was located directly under a single tree crown. For each of the 110 field plots with identifiable plot centers– the "validation field plots", we calculated 7 forest structure metrics using the ground data collected by Fettig et al. (2019): total number of trees, number of trees greater than 15 m in height, mean height of trees, 25th percentile tree height, 75th percentile tree height, mean distance to nearest tree neighbor, and mean distance to second nearest neighbor. For each tree detection algorithm and parameter set described above, we calculated the same set of 7 structure metrics within the footprint of the validation field plots. We calculated the Pearson's correlation and root mean square error (RMSE) between the ground data and the aerial data for each of the 7 structure metrics for each of the 177 automatic tree detection algorithms/parameter sets. For each algorithm and parameter set, we calculated its performance relative to other algorithms as whether its Pearson's correlation was within 5% of the highest Pearson's correlation as well as whether its RMSE was within 5% of the lowest RMSE. We summed the number of forest structure metrics for which it reached these 5% thresholds for each algorithm/parameter set. For automatically detecting trees across the whole study, we selected the algorithm/parameter set that performed well across the most number of forest metrics (see Results).

We delineated individual tree crowns (Figure 2; Level 3a, fourth image) with a marker controlled watershed segmentation algorithm (Meyer and Beucher 1990) implemented in the `ForestTools` package (Plowright

2018) using the detected treetops as markers. If the automatic segmentation algorithm failed to generate a crown segment for a detected tree (e.g., often snags with a very small crown footprint), a circular crown was generated with a radius of 0.5 m. If the segmentation generated multiple polygons for a single detected tree, only the polygon containing the detected tree was retained. Because image overlap decreases near the edges of the overall flight path and reduces the quality of the SfM processing in those areas, we excluded segmented crowns within 35 m of the edge of the survey area. Given the narrower field of view of the Rededge3 multispectral camera versus the X3 RGB camera whose optical parameters were used to define the ~40 ha survey area around each site, as well as the 35 m additional buffering, the survey area at each site was ~30 ha (see Supplemental Information).

Level 3b: Data derived from spectral AND geometric information

We overlaid the segmented crowns on the reflectance maps from 20 sites spanning the latitudinal and elevation gradient in the study. Using QGIS (https://qgis.org/en/site/), we hand classified 564 trees as live/dead (Figure 3) and as one of 5 dominant species in the study area (ponderosa pine, *Pinus lambertiana*, *Abies concolor*, *Calocedrus decurrens*, or *Quercus kelloggi*) using the mapped ground data as a guide. Each tree was further classified as "host" for ponderosa pine or "non-host" for all other species (Fettig 2016). We extracted all the pixel values within each segmented crown polygon from the five, Level 2 orthorectified reflectance maps (one per narrow band on the Rededge3 camera) as well as from the five, Level 3a vegetation index maps using the `velox` package (Hunziker 2017). For each crown polygon, we calculated the mean value of the extracted Level 2 and Level 3a pixels and used them as ten independent variables in a five-fold cross validated boosted logistic regression model to predict whether the hand classified trees were alive or dead. For just the living trees, we similarly used all 10 mean reflectance values per crown polygon to predict tree species using a five-fold cross validated regularized discriminant analysis. The boosted logistic regression and regularized discriminant analysis were implemented using the `caret` package in R (Kuhn 2008). We used these models to classify all tree crowns in the data set as alive or dead (Figure 2; Level 3b, first image) as well as the species of living trees (Figure 2; Level 3b, second image). Finally, we estimated the basal area of each tree from their photogrammetry-derived height using species-specific simple linear regressions of the relationship between height and DBH as measured in the coincident field plots from Fettig et al. (2019).

Level 4: Aggregations to regular grids

We rasterized the forest structure and composition data at a spatial resolution similar to that of the field plots to better match the grain size at which we validated the automatic tree detection algorithms. In each raster cell, we calculated: number of dead trees, number of ponderosa pine trees, total number of trees, and

mean height of ponderosa pine trees. The values of these variables in each grid cell and derivatives from them were used for visualization and modeling. Here, we show the fraction of dead trees per cell (Figure 2; Level 4, first image), the fraction of host trees per cell (Figure 2; Level 4, second image), the mean height of ponderosa pine trees in each cell (Figure 2; Level 4, third image), and the total count of trees per cell (Figure 2; Level 4, fourth image).

Note on assumptions about dead trees

For the purposes of this study, we assumed that all dead trees were ponderosa pine and thus hosts colonized by WPB. This is a reasonably good assumption for our study area; for example, Fettig et al. (2019) found that 73.4% of dead trees in their coincident field plots were ponderosa pine. Mortality was concentrated in the larger-diameter classes and attributed primarily to WPB (see Figure 5 of Fettig et al. 2019). The species contributing to the next highest proportion of dead trees was incense cedar which represented 18.72% of the dead trees in the field plots. While the detected mortality is most likely to be ponderosa pine killed by WPB, it is critical to interpret our results with these limitations in mind.

Environmental data

We used CWD (Stephenson 1998) from the 1981-2010 mean value of the basin characterization model (Flint et al. 2013) as an integrated measure of historic temperature and moisture conditions for each of the 32 sites. Higher values of CWD correspond to historically hotter, drier conditions and lower values correspond to historically cooler, wetter conditions. CWD has been shown to correlate well with broad patterns of tree mortality in the Sierra Nevada (Young et al. 2017) as well as bark beetle-induced tree mortality (Millar et al. 2012). The forests along the entire CWD gradient used in this study experienced exceptional hot drought between 2012 to 2015 with a severity of at least a 1,200-year event, and perhaps more severe than a 10,000-year event (Griffin and Anchukaitis 2014, Robeson 2015). We converted the CWD value for each site into a z-score representing that site's deviation from the mean CWD across the climatic range of Sierra Nevada ponderosa pine as determined from 179 herbarium records described in Baldwin et al. (2017). Thus, a CWD z-score of 1 would indicate that the CWD at that site is one standard deviation hotter/drier than the mean CWD across all geolocated herbarium records for ponderosa pine in the Sierra Nevada.

Statistical model

We used a generalized linear model with a zero-inflated binomial response and a logit link to predict the probability of ponderosa pine mortality within each 20 x 20-m cell using the total number of ponderosa pine trees in each cell as the number of trials, and the number of dead trees in each cell as the number of

14

³⁵⁶ "successes". As covariates, we used the proportion of trees that are WPB hosts (i.e., ponderosa pine) in each

³⁵⁷ cell, the mean height of ponderosa pine trees in each cell, the count of trees of all species (overall density) in

³⁵⁸ each cell, and the site-level CWD using Eq. 1. Note that the two-way interaction between the overall density

³⁵⁹ and the proportion of trees that are hosts is directly proportional to the number of ponderosa pine trees in

³⁶⁰ the cell. We centered and scaled all predictor values, and used weakly-regularizing default priors from the

³⁶¹ `brms` package (Bürkner 2017). To measure and account for spatial autocorrelation underlying ponderosa pine

³⁶² mortality, we subsampled the data at each site to a random selection of 200, 20 x 20-m cells representing

³⁶³ approximately 27.5% of the surveyed area. Additionally with these subsampled data, we included a separate

³⁶⁴ exact Gaussian process term per site of the noncentered/nonscaled interaction between the x- and y-position

³⁶⁵ of each cell using the `gp()` function in the `brms` package (Bürkner 2017). The Gaussian process estimates the

³⁶⁶ spatial covariance in the response variable (log-odds of ponderosa pine mortality) jointly with the effects of

³⁶⁷ the other covariates.

$$y_{i,j} \sim \begin{cases} 0, & p \\ Binom(n_i, \pi_i), & 1-p \end{cases}$$

$$logit(\pi_i) = \beta_0 +$$

$$\beta_1 X_{cwd,j} + \beta_2 X_{propHost,i} + \beta_3 X_{PipoHeight,i} +$$

$$\beta_4 X_{overallDensity,i} + \beta_5 X_{overallBA,i} +$$

$$\beta_6 X_{cwd,j} X_{PipoHeight,i} + \beta_7 X_{cwd,j} X_{propHost,i} +$$

$$\beta_8 X_{cwd,j} X_{overallDensity,i} + \beta_9 X_{cwd,j} X_{overallBA,i} +$$

$$\beta_10 X_{propHost,i} X_{PipoHeight,i} + \beta_11 X_{propHost,i} X_{overallDensity,i} +$$

$$\beta_{12} X_{cwd,j} X_{propHost,i} X_{PipoHeight,i} +$$

$$\mathcal{GP}_j(x_i, y_i)$$

³⁶⁸ Where y_i is the number of dead trees in cell i, n_i is the sum of the dead trees (assumed to be ponderosa pine)

³⁶⁹ and live ponderosa pine trees in cell i, π_i is the probability of ponderosa pine tree mortality in cell i, p is the

³⁷⁰ probability of there being zero dead trees in a cell arising as a result of an independent, unmodeled process,

³⁷¹ $X_{cwd,j}$ is the z-score of CWD for site j, $X_{propHost,i}$ is the scaled proportion of trees that are ponderosa pine

³⁷² in cell i, $X_{PipoHeight,i}$ is the scaled mean height of ponderosa pine trees in cell i, $X_{overallDensity,i}$ is the scaled

³⁷³ density of all trees in cell i, $X_{overallBA,i}$ is the scaled basal area of all trees in cell i, x_i and y_i are the x- and

³⁷⁴ y- coordinates of the centroid of the cell in an EPSG3310 coordinate reference system, and $\mathcal{GP}_j$ represents

₃₇₅ the exact Gaussian process describing the spatial covariance between cells at site j.

₃₇₆ We fit this model using the `brms` package (Bürkner 2017) which implements the No U-Turn Sampler extension
₃₇₇ to the Hamiltonian Monte Carlo algorithm (Hoffman and Gelman 2014) in the Stan programming language
₃₇₈ (Carpenter et al. 2017). We used 4 chains with 4000 iterations each (2000 warmup, 2000 samples), and
₃₇₉ confirmed chain convergence by ensuring all `Rhat` values were less than 1.1 (Brooks and Gelman 1998) and
₃₈₀ that the bulk and tail effective sample sizes (ESS) for each estimated parameter were greater than 100 times
₃₈₁ the number of chains (i.e., greater than 400 in our case). We used posterior predictive checks to visually
₃₈₂ confirm model performance by overlaying the density curves of the predicted number of dead trees per cell
₃₈₃ over the observed number (Gabry et al. 2019). For the posterior predictive checks, we used 50 random
₃₈₄ samples from the model fit to generate 50 density curves and ensured curves were centered on the observed
₃₈₅ distribution, paying special attention to model performance at capturing counts of zero.

Software and data availability

₃₈₇ All data are available via the Open Science Framework. Statistical analyses were performed using the `brms`
₃₈₈ packages. With the exception of the SfM software (Pix4Dmapper Cloud) and the GIS software QGIS, all
₃₈₉ data carpentry and analyses were performed using `R` (R Core Team 2018).

Results

Tree detection algorithm performance

₃₉₂ We found that the experimental `lmfx` algorithm with parameter values of `dist2d = 1` and `ws = 2.5` (Roussel
₃₉₃ et al. 2019) performed the best across 7 measures of forest structure as measured by Pearson's correlation
₃₉₄ with ground data (Table 2).

Table 2: Correlation and differences between the best performing tree detection algorithm (lmfx with dist2d = 1 and ws = 2.5) and the ground data. An asterisk next to the correlation or RMSE indicates that this value was within 5% of the value of the best-performing algorithm/parameter set. Ground mean represents the mean value of the forest metric across the 110 field plots that were visible from the sUAS-derived imagery. The median error is calculated as the median of the differences between the air and ground values for the 110 visible plots. Thus, a positive number indicates an overestimate by the sUAS workflow and a negative number indicates an underestimate.

Forest structure metric	Ground mean	Correlation with ground	RMSE	Median error
total tree count	19	0.67*	8.68*	2
count of trees > 15 m	9.9	0.43	7.38	0
distance to 1st neighbor (m)	2.8	0.55*	1.16*	0.26

Forest structure metric	Ground mean	Correlation with ground	RMSE	Median error
distance to 2nd neighbor (m)	4.3	0.61*	1.70*	0.12
height (m); 25th percentile	12	0.16	8.46	-1.2
height (m); mean	18	0.29	7.81*	-2.3
height (m); 75th percentile	25	0.35	10.33*	-4

Classification accuracy for live/dead and host/non-host

The accuracy of live/dead classification on a withheld test dataset was 96.4%. The accuracy of species classification on a withheld testing dataset was 64.1%. The accuracy of WPB host/non-WPB-host (i.e., ponderosa pine versus other tree species) on a withheld testing dataset was 71.8%.

Site summary based on best tree detection algorithm and classification

Across all study sites, we detected, segmented, and classified 452,413 trees. Of these trees, we classified 118,879 as dead (26.3% mortality). Estimated site-level tree mortality ranged from 6.8% to 53.6%. See Supplemental Information for site summaries and comparisons to site-level mortality measured from field data.

Effect of local structure and regional climate on tree mortality attributed to western pine beetle

Site-level CWD exerted a positive, but relatively weak, main effect on the probability of ponderosa mortality (effect size: 0.16; 95% CI: [0.03, 0.30]; Figure 4). We found a positive main effect of proportion of host trees per cell (effect size: 0.76; 95% CI: [0.70, 0.82]), with a greater proportion of host trees (i.e., ponderosa pine) in a cell increasing the probability of ponderosa pine mortality. We detected no effect of overall tree density nor overall basal area (i.e., including both ponderosa pine and non-host species; tree density effect size: -0.05; 95% CI: [-0.13, 0.03]; basal area effect size: 0.00; 95% CI: [-0.11, 0.11]).

We found a positive two-way interaction between the overall tree density per cell and the proportion of trees that were hosts, which is equivalent to a positive effect of the density of host trees (effect size: 0.08; 95% CI: [0.03, 0.13]; Figure 4).

We found a negative effect of mean height of ponderosa pine on the probability of ponderosa mortality, suggesting that WPB attacked smaller trees, on average (effect size: -0.40; 95% CI: [-0.50, -0.30]). However, there was a positive interaction between CWD and ponderosa pine mean height, such that larger trees were
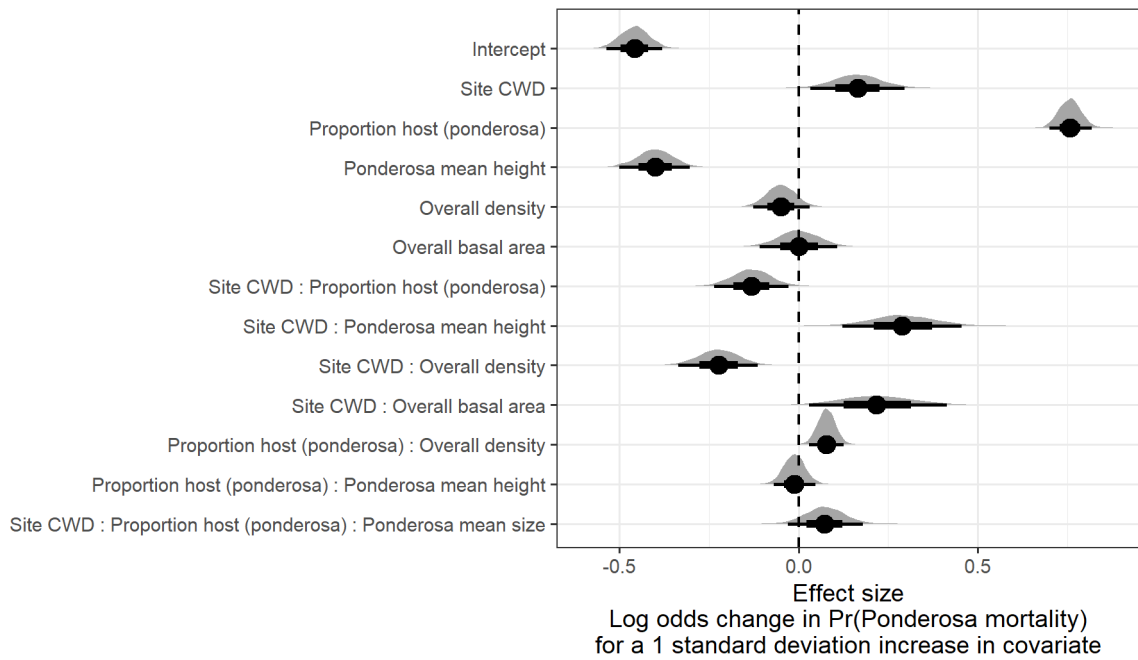
17

Figure 4: Posterior distributions of effect size from zero-inflated binomial model predicting the probability of ponderosa pine mortality in a 20 x 20-m cell given forest structure characteristics and site-level climatic water deficit (CWD). The gray filled area for each model covariate represents the probability density of the posterior distribution, the point underneath each density curve represents the median of the estimate, the bold interval surrounding the point estimate represents the 66% credible interval, and the thin interval surrounding the point estimate represents the 95% credible interval.

more likely to increase the local probability of ponderosa mortality in hotter, drier sites (effect size: 0.29; 95% CI: [0.12, 0.46]; Figure 5).

We found weakly negative effects of the site-level CWD interactions with both the proportion of host trees and overall tree density (CWD/proportion host interaction effect size: -0.13; 95% CI: [-0.23, -0.03]; Figure 4; CWD/overall tree density interaction effect size: -0.22; 95% CI: [-0.34, -0.11]; Figure 4; Figure 5). We found a positive effect of the interaction between CWD and total basal area (effect size: 0.22; 95% CI: [0.03, 0.42]; Figure 4; Figure 5).
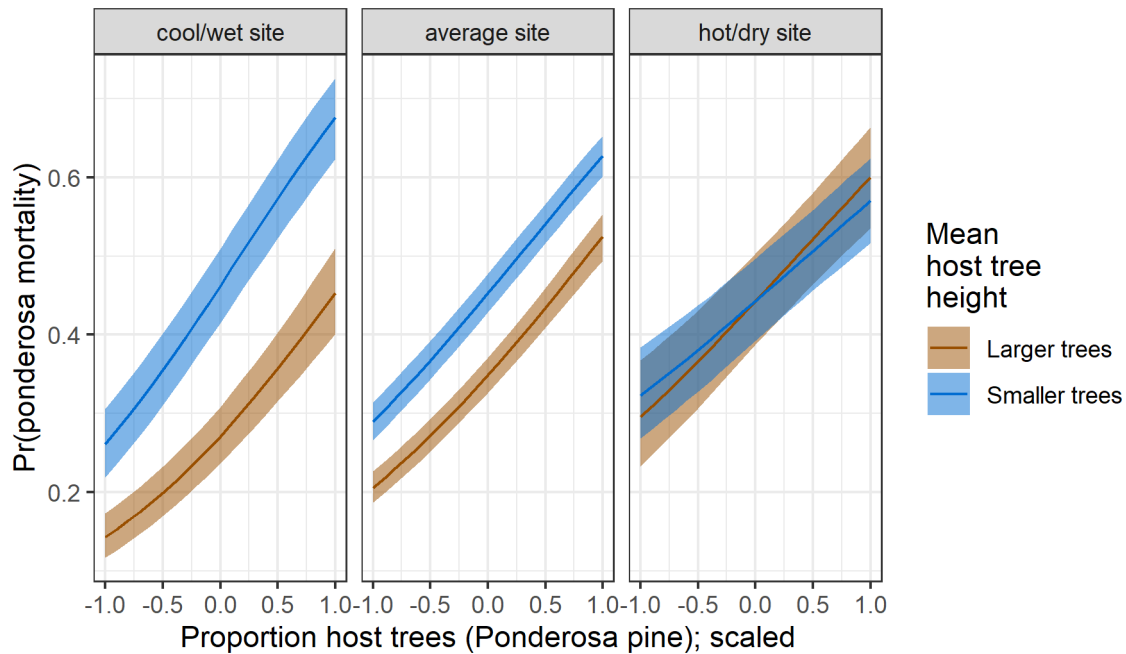

Figure 5: Line version of model results with 95% credible intervals showing primary influence of ponderosa pine structure on the probability of ponderosa pine mortality, and the interaction across climatic water deficit. The 'larger trees' line represents the mean height of ponderosa pine 0.7 standard deviations above the mean (approximately 24.1 m), and the 'smaller trees' line represents the mean height of ponderosa pine 0.7 standard deviations below the mean (approximately 12.1 m).

Discussion

This study represents a novel use of drones to refine our understanding of the patterns of tree mortality following the 2012 to 2015 California hot drought and its aftermath. By simultaneously measuring the effects of local forest structure and composition with broad-scale environmental gradients, we were able to better characterize the disturbance amplifying effect of a tree-killing insect, the WPB, compared to using correlates of tree stress alone.

Weak positive main effect of CWD

We found only a relatively weak positive effect of site-level CWD on ponderosa pine mortality rate. To that end, we did not measure tree water stress at an individual tree level as in other recent work (Stephenson et al. 2019), and instead treated CWD as a general indicator of tree stress following results of coarser-scale studies (e.g., Young et al. 2017), which may have contributed to our failure to detect a stronger CWD effect. When measured at a fine scale, even if not at an individual tree level, progressive canopy water loss can be a good indicator of tree water stress and increased vulnerability to mortality from drought or bark beetles (Brodrick and Asner 2017). Our entire study area experienced exceptional hot drought between 2012 and 2015 (Griffin and Anchukaitis 2014, Robeson 2015) and the variation of mortality explained by a main effect of CWD may be dampened when most trees are experiencing a high degree of water stress (Floyd et al. 2009, Fettig et al. 2019). Importantly, using a 30-year historic average of CWD as a site-level indicator of tree stress doesn't allow us to disentangle whether water availability was lower in an absolute sense during the drought or whether increasing tree vulnerability to bark beetles was driven by chronic water stress at these historically hotter/drier sites (McDowell et al. 2008).

Positive effect of host density and a negative effect of overall density

A number of mechanisms associated with the relative abundance of species in a local area might underlie the strong effect of host proportion on the probability of host tree mortality. Frequency-dependent herbivory– whereby mixed-species forests experience less herbivory compared to monocultures (as an extreme example)– is common, especially for oligophagous insect species (Jactel and Brockerhoff 2007). Nonhost volatiles reduce attraction of several species of bark beetles to their aggregation pheromones (Seybold et al. 2018), including WPB (Fettig et al. 2005). Combinations of nonhost volatiles and an antiaggregation pheromone have been used successfully to reduce levels of tree mortality attributed to WPB in California (e.g., Fettig et al. 2008, 2012). Hayes et al. (2009) and Fettig et al. (2019) found that measures of host availability explained less variation in mortality than measures of overall tree density. Those conclusions, however, were based on a response variable of "total number of dead host trees," rather than the number of dead host trees conditional on the total number of host trees as in our study (i.e., a binomial response).

The negative relationship between overall tree density and the probability of ponderosa pine mortality corroborates findings of coincident ground plots (Fettig et al. 2019, in their analysis using proportion of trees killed as a response) and other work during the same hot drought (Restaino et al. 2019). In the absence of management, forest structure is largely a product of climate and, with increasing importance at finer spatial scales, topographic conditions (Fricker et al. 2019). Denser forest patches in our study may indicate greater

20

local water availability, more favorable conditions for tree growth and survivorship, and increased resistance to beetle-induced tree mortality (Ma et al. 2010, Restaino et al. 2019, Fricker et al. 2019). The negative two-way interaction between site CWD and overall density that amplifies the negative overall density effect in hotter, drier sites (effect size: -0.22; 95% CI: [-0.34, -0.11]) supports this explanation if greater local tree density implies especially favorable growing conditions (and locally resistant trees) when denser patches are found in hot, dry sites.

The positive relationship between host density and susceptibility to colonization by bark beetles has been so well-documented at the experimental plot level (e.g., Raffa and Berryman 1987, Oliver 1995) that lowering stand densities through selective harvest of hosts is commonly recommended for reducing future levels of tree mortality attributed to bark beetles (Fettig and Hilszczański 2015), including WPB (Fettig 2016). Greater host density shortens the flight distance required for WPB to disperse to new hosts, which likely facilitates bark beetle spread, however we calibrated our aerial tree detection to ~400 m^2 areas rather than to individual tree locations, so our data are insufficient to address these relationships. Increased density of ponderosa pine, specifically, may disproportionately increase the competitive environment for host trees (and thus increase their susceptibility to WPB colonization) if intraspecific competition amongst ponderosa pine trees is stronger than interspecific competition as would be predicted with coexistence theory (Chesson 2000). Finally, greater host densities increase the frequency that searching WPB land on hosts, rather than nonhosts, thus reducing the amount of energy expended during host finding and selection as well as the time that searching WPB spend exposed to a variety of predators outside the host tree.

Positive interaction effect of CWD and basal area

While overall tree density is likely an indicator of favorable microsites in fire-suppressed forests, overall basal area is a better indicator of the local competitive environment especially in water-limited forests (Ma et al. 2010, Fricker et al. 2019). While we found no main effect of overall basal area on the probability of ponderosa mortality, we did detect a clear interaction between site-level CWD and basal area such that mortality rates of ponderosa pine in hotter, drier sites were greater when local overall basal area was high. This is a similar interaction as found by Young et al. (2017), and we perhaps did not detect a similar main effect of basal area as Young et al. (2017) because we partitioned this overall effect into the influence of finer-scale forest structure and composition (e.g., number of host trees).

Negative main effect of host tree mean size, but strong positive interaction with site CWD

The negative main effect of host tree mean size was surprising, and appears to contradict long-standing wisdom on the dynamics of WPB in the Sierra Nevada. WPB exhibit a preference for trees 50.8 to 76.2 cm DBH (Person 1928, 1931), and a positive relationship between host tree size and levels of tree mortality attributed to WPB was reported by Fettig et al. (2019) in the coincident field plots as well as in other recent studies (Restaino et al. 2019, Stephenson et al. 2019, Pile et al. 2019). Indeed, Fettig et al. (2019) attributed no mortality to WPB in ponderosa pine trees <10.0 cm DBH and found no tree size/mortality relationship for incense cedar or white fir in the coincident field plots. These species represent 22.3% of the total tree mortality observed in their study, yet in our study all dead trees were classified as ponderosa pine (see Methods) which could dampen the positive effect of tree size on tree mortality. Larger trees are more nutritious and are therefore ideal targets if local bark beetle density is high enough to successfully initiate mass attack and overwhelm tree defenses, as can occur when many trees are under severe water stress (Bentz et al. 2010, Boone et al. 2011, Kolb et al. 2016). In the recent hot drought, we expected that most trees would be under severe water stress, setting the stage for increasing beetle density, successful mass attacks, and targeting of larger trees. A possible explanation for our finding counter to this expectation is that our observations represent the cumulative mortality of trees during a multi-year drought event and its aftermath. Lower host tree mean size led to a greater probability of host mortality earlier in this drought (Pile et al. 2019, Stovall et al. 2019) and that signal might have persisted even as mortality continued to accumulate driven by other factors. Another explanation may be that our extensive sampling design better captured the contagious process by which bark beetles colonize smaller, suboptimal trees in the vicinity of the larger, more desirable trees that are the focus of initial attack (e.g., Klein et al. 1978). If larger, desirable trees tend to be associated with a greater local density of smaller trees that are also colonized in this contagious process, then we might observe a negative relationship between tree size and ponderosa mortality rates. Finally, tree growth rates may be a better predictor of susceptibility to WPB colonization than tree size per se, with slower-growing trees being most vulnerable (Miller and Keen 1960). While slow-growing trees are often also the largest trees, this may not be the case for our study sites especially given the legacy of fire suppression in the Sierra Nevada and its effect of perturbing forest structure far outside its natural range of variation (Safford and Stevens 2017).

In hot, dry sites, larger average host size increased the probability of host mortality while smaller host sizes increased the probability of host mortality in cooler, wetter sites. Notably, a similar pattern was shown by Stovall et al. (2019) with a strong positive tree height/mortality relationship in areas with the greatest vapor pressure deficit and no tree height/mortality relationship in areas with the lowest vapor pressure

22

deficit. Stovall et al. (2019) did not observe that this environmental dependence extended to a negative tree height/mortality relationship (as we did) even at the lowest extremes of their vapor pressure deficit gradient, perhaps because their entire study took place in the southern Sierra Nevada which represents a hotter, drier portion of the more spatially extensive results we present here. Our work suggests that the WPB was cueing into different aspects of forest structure across an environmental gradient in a spatial context in a parallel manner to the temporal context noted by Stovall et al. (2019) and Pile et al. (2019), who observed that mortality was increasingly driven by larger trees as the hot drought proceeded and became more severe.

All of our sites were considered in an "epidemic" population phase for WPB (>5 trees killed per ha; see Supplemental Information; Miller and Keen 1960, Hayes et al. 2009), but our results challenge the notion that outbreak behavior by the WPB and subsequent tree mortality is always driven by greater tree size. Despite a strong tree size/mortality relationship in coincident ground plots across our study area (Fettig et al. 2019), our results from surveying the broader context surrounding those ground plots reveals different effects of host tree size depending on CWD. Thus, it is possible that the massive tree mortality in hotter/drier Sierra Nevada forests (lower latitudes and elevations; Asner et al. 2016, Young et al. 2017) during the 2012 to 2015 hot drought arose as a synergistic alignment of environmental conditions and local forest structure that allowed WPB to successfully colonize large trees, rapidly increase in population size, and expand. The unexpectedly low mortality in cooler/wetter Sierra Nevada forests compared to model predictions based on coarser-scale forest structure data (Young et al. 2017) may result from a different WPB response to local forest structure due to a lack of an alignment with favorable climate conditions.

Limitations and future directions

We have demonstrated that drones can be effective means of collecting forest data at multiple, vastly different spatial scales to investigate a single, multi-scale phenomenon– from meters in between trees, to hundreds of meters of elevation, to hundreds of thousands of meters of latitude. Some limitations remain, but can be overcome with further refinements in the use of this tool for forest ecology. Most of these limitations arise from tree detection and classification uncertainty, making it imperative to work with field data for calibration and uncertainty reporting.

The greatest limitation in our study arising from classification uncertainty is in the assumption that all dead trees were ponderosa pine, which we estimate from coincident field plots is true approximately 73.4% of the time. Because the forest structure factors influencing the likelihood of individual tree mortality during the hot drought depended on tree species (Stephenson et al. 2019), we cannot rule out that some of the ponderosa pine mortality relationships to forest structure that we observed may be partially explained by

those relationships in other species that were misclassified as ponderosa pine using our methods. However, the overall community composition across our study area was similar (Fettig et al. 2019) and we are able to reproduce similar forest structure/mortality patterns in drone-derived data when restricting the scope of analysis to only trees detected in the footprints of the coincident field plots, but with dramatically different patterns observed when including data from the forest surrounding the coincident field plots (see Supplemental information). Thus, we remain confident that the patterns we observed were driven primarily by the dynamic between WPB and ponderosa pine. While spectral information of foliage could help classify living trees to species, the species of standing dead trees were not spectrally distinct. This challenge of classifying standing dead trees to species implies that a conifer forest system with less bark beetle and tree host diversity, such as mountain pine beetle outbreaks in monocultures of lodgepole pine in the Intermountain West, should be particularly amenable to the methods presented here even with minimal further refinement because dead trees will almost certainly belong to a single species and have succumbed to colonization by a single bark beetle species.

Some uncertainty surrounded our ability to detect trees using the geometry of the dense point clouds derived with SfM. The horizontal accuracy of the tree detection was better than the vertical accuracy, which may result from a more significant error contribution by the field-based calculations of tree height compared to tree position relative to plot center (Table 2). Both the horizontal and vertical accuracy would likely improve with better SfM point clouds, which can be enhanced with greater overlap between images (Frey et al. 2018) or with oblique (i.e., off-nadir) imagery (James and Robson 2014). Frey et al. (2018) found that 95% overlap was preferable for generating dense point clouds in forested areas, and James and Robson (2014) reduced dense point cloud errors using imagery taken at 30 degrees off-nadir. We only achieved 91.6% overlap with the X3 RGB camera and 83.9% overlap with the multispectral camera, and all imagery was nadir-facing. While our live/dead classification was fairly accurate (96.4% on a withheld dataset), our species classifier would likely benefit from better crown segmentation because the pixel-level reflectance values within each crown are averaged to characterize the "spectral signature" of each tree. With better delineation of each tree crown, the mean value of pixels within each tree crown will likely be more representative of that tree's spectral signature. Better crown segmentation might most readily be achieved through greater overlap in imagery. We anticipate that computer vision and deep learning will prove helpful in overcoming some of these detection and classification challenges (Gray et al. 2019).

Finally, we note our study is constrained by using the probability of ponderosa mortality as our key response variable. This measure is well-suited to understanding the dynamics between WPB colonization behavior and host tree susceptibility, but may not capture impacts on the forest ecosystem and its services as well as a

24

measure of biomass reduction such as tree basal area.

Conclusions

Climate change adaptation strategies emphasize management action that considers whole-ecosystem responses to inevitable change (Millar et al. 2007), which requires a macroecological understanding of how phenomena at multiple scales can interact. Tree vulnerability to environmental stressors presents only a partial explanation for tree mortality patterns during hot droughts, especially when bark beetles are present. We've shown that drones can be a valuable tool for investigating multi-scalar phenomena, such as how local forest structure combines with environmental conditions to shape forest insect disturbance. Understanding the conditions that drive dry western U.S. forest responses to disturbances such as bark beetle outbreaks will be vital for predicting outcomes from increasing disturbance frequency and intensity exacerbated by climate change (Vose et al. 2018). Our study suggests that outcomes will depend on interactions between local forest structure and broad-scale environmental gradients, with the potential for cross-scale interactions to enhance our understanding of forest insect dynamics.

References

Anderegg, W. R. L., J. A. Hicke, R. A. Fisher, C. D. Allen, J. Aukema, B. Bentz, S. Hood, J. W. Lichstein, A. K. Macalady, N. McDowell, Y. Pan, K. Raffa, A. Sala, J. D. Shaw, N. L. Stephenson, C. Tague, and M. Zeppel. 2015. Tree mortality from drought, insects, and their interactions in a changing climate. New Phytologist 208:674–683.

Asner, G. P., P. G. Brodrick, C. B. Anderson, N. Vaughn, D. E. Knapp, and R. E. Martin. 2016. Progressive forest canopy water loss during the 2012-2015 California drought. Proceedings of the National Academy of Sciences 113:E249–E255.

Baldwin, B. G., A. H. Thornhill, W. A. Freyman, D. D. Ackerly, M. M. Kling, N. Morueta-Holme, and B. D. Mishler. 2017. Species richness and endemism in the native flora of California. American Journal of Botany 104:487–501.

Bedard, W. D., P. E. Tilden, D. L. Wood, R. M. Silverstein, R. G. Brownlee, and J. O. Rodin. 1969. Western pine beetle: Field response to its sex pheromone and a synergistic host terpene, myrcene. Science 164:1284–1285.

Bentz, B. J., J. Régnière, C. J. Fettig, E. M. Hansen, J. L. Hayes, J. A. Hicke, R. G. Kelsey, J. F. Negrón, and S. J. Seybold. 2010. Climate change and bark beetles of the western United States and Canada: Direct and indirect effects. BioScience 60:602–613.

Berryman, A. A. 1982. Population dynamics of bark beetles. Pages 264–314 *in* Bark Beetles in North American Conifers: A System for the Study of Evolutionary Biology.

Boone, C. K., B. H. Aukema, J. Bohlmann, A. L. Carroll, and K. F. Raffa. 2011. Efficacy of tree defense physiology varies with bark beetle population density: A basis for positive feedback in eruptive species. Canadian Journal of Forest Research 41:1174–1188.

Brodrick, P. G., and G. P. Asner. 2017. Remotely sensed predictors of conifer tree mortality during severe drought. Environmental Research Letters 12:115013.

Brooks, S. P., and A. Gelman. 1998. General methods for monitoring convergence of iterative simulations. Journal of Computational and Graphical Statistics 7:434.

Bürkner, P.-C. 2017. **brms**: An *R* package for bayesian multilevel models using *Stan*. Journal of Statistical Software 80:1–28.

Byers, J. A., and D. L. Wood. 1980. Interspecific inhibition of the response of the bark beetles, *Dendroctonus*

brevicomis and *Ips paraconfusus*, to their pheromones in the field. Journal of Chemical Ecology 6:149–164.

Carpenter, B., A. Gelman, M. D. Hoffman, D. Lee, B. Goodrich, M. Betancourt, M. Brubaker, J. Guo, P. Li, and A. Riddell. 2017. Stan: A Probabilistic Programming Language. Journal of Statistical Software 76:1–32.

Chesson, P. 2000. Mechanisms of maintenance of species diversity. Annual Review of Ecology and Systematics 31:343–366.

Chubaty, A. M., B. D. Roitberg, and C. Li. 2009. A dynamic host selection model for mountain pine beetle, *Dendroctonus ponderosae* Hopkins. Ecological Modelling 220:1241–1250.

Clevers, J., and A. Gitelson. 2013. Remote estimation of crop and grass chlorophyll and nitrogen content using red-edge bands on Sentinel-2 and -3. International Journal of Applied Earth Observation and Geoinformation 23:344–351.

Coops, N. C., M. Johnson, M. A. Wulder, and J. C. White. 2006. Assessment of QuickBird high spatial resolution imagery to detect red attack damage due to mountain pine beetle infestation. Remote Sensing of Environment 103:67–80.

DJI. 2015a. Zenmuse X3 - Creativity Unleashed. https://www.dji.com/zenmuse-x3/info.

DJI. 2015b. DJI - The World Leader in Camera Drones/Quadcopters for Aerial Photography. https://www.dji.com/matrice100/info.

DronesMadeEasy. 2018. Map Pilot for DJI on iOS. https://itunes.apple.com/us/app/map-pilot-for-dji/id1014765000?mt=8.

Evenden, M. L., C. M. Whitehouse, and J. Sykes. 2014. Factors influencing flight capacity of the mountain pine beetle (Coleoptera: Curculionidae: Scolytinae). Environmental Entomology 43:187–196.

Eysn, L., M. Hollaus, E. Lindberg, F. Berger, J.-M. Monnet, M. Dalponte, M. Kobal, M. Pellegrini, E. Lingua, D. Mongus, and N. Pfeifer. 2015. A benchmark of LiDAR-based single tree detection methods using heterogeneous forest data from the alpine space. Forests 6:1721–1747.

Farr, T. G., P. A. Rosen, E. Caro, R. Crippen, R. Duren, S. Hensley, M. Kobrick, M. Paller, E. Rodriguez, L. Roth, D. Seal, S. Shaffer, J. Shimada, J. Umland, M. Werner, M. Oskin, D. Burbank, and D. Alsdorf. 2007. The shuttle radar topography mission. Reviews of Geophysics 45.

Fettig, C. J. 2012. Chapter 2: Forest health and bark beetles. *in* Managing Sierra Nevada Forests. PSW-GTR-237. USDA Forest Service.

Fettig, C. J. 2016. Native bark beetles and wood borers in Mediterranean forests of California. Pages 499–528 *in* Insects and diseases of Mediterranean Forest systems. Springer International Publishing, Switzerland.

Fettig, C. J., C. P. Dabney, S. R. McKelvey, and D. P. W. Huber. 2008. Nonhost angiosperm volatiles and verbenone protect individual ponderosa pines from attack by western pine beetle and red turpentine beetle (Coleoptera: Curculionidae, Scolytinae). Western Journal of Applied Forestry 23:40–45.

Fettig, C. J., and J. Hilszczański. 2015. Management strategies for bark beetles in conifer forests. Pages 555–584 *in* Bark Beetles. Elsevier.

Fettig, C. J., K. D. Klepzig, R. F. Billings, A. S. Munson, T. E. Nebeker, J. F. Negrón, and J. T. Nowak. 2007. The effectiveness of vegetation management practices for prevention and control of bark beetle infestations in coniferous forests of the western and southern United States. Forest Ecology and Management 238:24–53.

Fettig, C. J., S. R. McKelvey, C. P. Dabney, D. P. W. Huber, C. G. Lait, D. L. Fowler, and J. H. Borden. 2012. Efficacy of "Verbenone Plus" for protecting ponderosa pine trees and stands from *Dendroctonus brevicomis* (Coleoptera: Curculionidae) attack in British Columbia and California. Journal of Economic Entomology 105:1668–1680.

Fettig, C. J., S. R. McKelvey, and D. P. W. Huber. 2005. Nonhost angiosperm volatiles and Verbenone disrupt response of western pine beetle, *Dendroctonus brevicomis* (Coleoptera: Scolytidae), to attractant-baited traps. Journal of Economic Entomology 98:2041–2048.

Fettig, C. J., L. A. Mortenson, B. M. Bulaon, and P. B. Foulk. 2019. Tree mortality following drought in the central and southern Sierra Nevada, California, U.S. Forest Ecology and Management 432:164–178.

Flint, L. E., A. L. Flint, J. H. Thorne, and R. Boynton. 2013. Fine-scale hydrologic modeling for regional landscape applications: The California Basin Characterization Model development and performance. Ecological Processes 2:25.

Floyd, M. L., M. Clifford, N. S. Cobb, D. Hanna, R. Delph, P. Ford, and D. Turner. 2009. Relationship of stand characteristics to drought-induced mortality in three Southwestern piñonJuniper woodlands. Ecological Applications 19:1223–1230.

Franceschi, V. R., P. Krokene, E. Christiansen, and T. Krekling. 2005. Anatomical and chemical defenses of conifer bark against bark beetles and other pests. New Phytologist 167:353–376.

Frey, J., K. Kovach, S. Stemmler, and B. Koch. 2018. UAV photogrammetry of forests as a vulnerable process. A sensitivity analysis for a structure from motion RGB-image pipeline. Remote Sensing 10:912.

Fricker, G. A., N. W. Synes, J. M. Serra-Diaz, M. P. North, F. W. Davis, and J. Franklin. 2019. More than climate? Predictors of tree canopy height vary with scale in complex terrain, Sierra Nevada, CA (USA). Forest Ecology and Management 434:142–153.

Gabry, J., D. Simpson, A. Vehtari, M. Betancourt, and A. Gelman. 2019. Visualization in Bayesian workflow. Journal of the Royal Statistical Society: Series A (Statistics in Society) 182:389–402.

Geiszler, D. R., and R. I. Gara. 1978. Mountain pine beetle attack dynamics in lodgepole pine. *in* Theory and Practice of Mountain Pine Beetle Management in Lodgepole Pine Forests: Symposium Proceedings. A. A. Berryman, G. D. Amman and R. W. Stark (Eds). Pullman, WA, USA.

Gitelson, A., and M. N. Merzlyak. 1994. Spectral reflectance changes associated with autumn senescence of *Aesculus hippocastanum* L. And *Acer platanoides* L. Leaves. Spectral features and relation to chlorophyll estimation. Journal of Plant Physiology 143:286–292.

Graf, M., M. Reid, B. Aukema, and B. Lindgren. 2012. Association of tree diameter with body size and lipid content of mountain pine beetles. The Canadian Entomologist 144:467–477.

Gray, P. C., A. B. Fleishman, D. J. Klein, M. W. McKown, V. S. Bézy, K. J. Lohmann, and D. W. Johnston. 2019. A convolutional neural network for detecting sea turtles in drone imagery. Methods in Ecology and Evolution 10:345–355.

Griffin, D., and K. J. Anchukaitis. 2014. How unusual is the 2012-2014 California drought? Geophysical Research Letters 41:9017–9023.

Hayes, C. J., C. J. Fettig, and L. D. Merrill. 2009. Evaluation of multiple funnel traps and stand characteristics for estimating western pine beetle-caused tree mortality. Journal of Economic Entomology 102:2170–2182.

Hijmans, R. J., J. van Etten, M. Sumner, J. Cheng, A. Bevan, R. Bivand, L. Busetto, M. Canty, D. Forrest, A. Ghosh, D. Golicher, J. Gray, J. A. Greenberg, P. Hiemstra, I. for M. A. Geosciences, C. Karney, M. Mattiuzzi, S. Mosher, J. Nowosad, E. Pebesma, O. P. Lamigueiro, E. B. Racine, B. Rowlingson, A. Shortridge, B. Venables, and R. Wueest. 2019. Raster: Geographic data analysis and modeling.

Hoffman, M. D., and A. Gelman. 2014. The No-U-Turn Sampler: Adaptively setting path lengths in Hamiltonian Monte Carlo. Journal of Machine Learning Research 15:31.

Hunziker, P. 2017. Velox: Fast raster manipulation and extraction.

Jactel, H., and E. G. Brockerhoff. 2007. Tree diversity reduces herbivory by forest insects. Ecology Letters 10:835–848.

Jakubowski, M. K., W. Li, Q. Guo, and M. Kelly. 2013. Delineating individual trees from LiDAR data: A comparison of vector- and raster-based segmentation approaches. Remote Sensing 5:4163–4186.

James, M. R., and S. Robson. 2014. Mitigating systematic error in topographic models derived from UAV and ground-based image networks. Earth Surface Processes and Landforms 39:1413–1420.

Jeronimo, S. M. A., V. R. Kane, D. J. Churchill, J. A. Lutz, M. P. North, G. P. Asner, and J. F. Franklin. 2019. Forest structure and pattern vary by climate and landform across active-fire landscapes in the montane Sierra Nevada. Forest Ecology and Management 437:70–86.

Kaiser, K. E., B. L. McGlynn, and R. E. Emanuel. 2013. Ecohydrology of an outbreak: Mountain pine beetle impacts trees in drier landscape positions first. Ecohydrology 6:444–454.

Kane, V. R., M. P. North, J. A. Lutz, D. J. Churchill, S. L. Roberts, D. F. Smith, R. J. McGaughey, J. T. Kane, and M. L. Brooks. 2014. Assessing fire effects on forest spatial structure using a fusion of Landsat and airborne LiDAR data in Yosemite National Park. Remote Sensing of Environment 151:89–101.

Klein, W. H., D. L. Parker, and C. E. Jensen. 1978. Attack, emergence, and stand depletion trends of the mountain pine beetle in a lodgepole pine stand during an outbreak. Environmental Entomology 7:732–737.

Kolb, T. E., C. J. Fettig, M. P. Ayres, B. J. Bentz, J. A. Hicke, R. Mathiasen, J. E. Stewart, and A. S. Weed. 2016. Observed and anticipated impacts of drought on forest insects and diseases in the United States. Forest Ecology and Management 380:321–334.

Kuhn, M. 2008. Building predictive models in R using the caret package. Journal of Statistical Software 28:1–26.

Larson, A. J., and D. Churchill. 2012. Tree spatial patterns in fire-frequent forests of western North America, including mechanisms of pattern formation and implications for designing fuel reduction and restoration treatments. Forest Ecology and Management 267:74–92.

Li, W., Q. Guo, M. K. Jakubowski, and M. Kelly. 2012. A new method for segmenting individual trees from the LiDAR point cloud. Photogrammetric Engineering & Remote Sensing 78:75–84.

Logan, J. A., P. White, B. J. Bentz, and J. A. Powell. 1998. Model analysis of spatial patterns in mountain pine beetle outbreaks. Theoretical Population Biology 53:236–255.

Ma, S., A. Concilio, B. Oakley, M. North, and J. Chen. 2010. Spatial variability in microclimate in a mixed-conifer forest before and after thinning and burning treatments. Forest Ecology and Management 259:904–915.

McDowell, N., W. T. Pockman, C. D. Allen, D. D. Breshears, N. Cobb, T. Kolb, J. Plaut, J. Sperry, A. West, D. G. Williams, and E. A. Yepez. 2008. Mechanisms of plant survival and mortality during drought: Why do some plants survive while others succumb to drought? New Phytologist 178:719–739.

Meyer, F., and S. Beucher. 1990. Morphological segmentation. Journal of Visual Communication and Image Representation 1:21–46.

Micasense. 2015. MicaSense. https://support.micasense.com/hc/en-us/articles/215261448-RedEdge-User-Manual-PDF-Download-.

Millar, C. I., N. L. Stephenson, and S. L. Stephens. 2007. Climate change and forests of the future: Managing in the face of uncertainty. Ecological Applications 17:2145–2151.

Millar, C. I., R. D. Westfall, D. L. Delany, M. J. Bokach, A. L. Flint, and L. E. Flint. 2012. Forest mortality in high-elevation whitebark pine (*Pinus albicaulis*) forests of eastern California, USA: Influence of environmental context, bark beetles, climatic water deficit, and warming. Canadian Journal of Forest Research 42:749–765.

Miller, J. M., and F. P. Keen. 1960. Biology and control of the western pine beetle: A summary of the first fifty years of research. US Department of Agriculture.

Mitchell, R. G., and H. K. Preisler. 1991. Analysis of spatial patterns of lodgepole pine attacked by outbreak populations of the mountain pine beetle. Forest Science 37:1390–1408.

Moeck, H. A., D. L. Wood, and K. Q. Lindahl. 1981. Host selection behavior of bark beetles (Coleoptera: Scolytidae) attacking *Pinus ponderosa*, with special emphasis on the western pine beetle, *Dendroctonus brevicomis*. Journal of Chemical Ecology 7:49–83.

Morris, J. L., S. Cottrell, C. J. Fettig, W. D. Hansen, R. L. Sherriff, V. A. Carter, J. L. Clear, J. Clement, R. J. DeRose, J. A. Hicke, P. E. Higuera, K. M. Mattor, A. W. R. Seddon, H. T. Seppä, J. D. Stednick, and S. J. Seybold. 2017. Managing bark beetle impacts on ecosystems and society: Priority questions to motivate future research. Journal of Applied Ecology 54:750–760.

Oliver, W. W. 1995. Is self-thinning in ponderosa pine ruled by *Dendroctonus* bark beetles? Page 6 *in* Forest health through silviculture: Proceedings of the 1995 National Silviculture Workshop.

Pau, G., F. Fuchs, O. Sklyar, M. Boutros, and W. Huber. 2010. EBImage: An R package for image processing with applications to cellular phenotypes. Bioinformatics 26:979–981.

Person, H. L. 1928. Tree selection by the western pine beetle. Journal of Forestry 26:564–578.

Person, H. L. 1931. Theory in explanation of the selection of certain trees by the western pine beetle. Journal

771 of Forestry 29:696–699.

772 Pile, L. S., M. D. Meyer, R. Rojas, O. Roe, and M. T. Smith. 2019. Drought impacts and compounding

773 mortality on forest trees in the southern Sierra Nevada. Forests 10:237.

774 Plowright, A. 2018. ForestTools: Analyzing remotely sensed forest data.

775 Preisler, H. K. 1993. Modelling spatial patterns of trees attacked by bark-beetles. Applied Statistics 42:501.

776 Raffa, K. F., B. H. Aukema, B. J. Bentz, A. L. Carroll, J. A. Hicke, M. G. Turner, and W. H. Romme. 2008.

777 Cross-scale drivers of natural disturbances prone to anthropogenic amplification: The dynamics of bark beetle

778 eruptions. BioScience 58:501–517.

779 Raffa, K. F., and A. A. Berryman. 1983. The role of host plant resistance in the colonization behavior and

780 ecology of bark beetles (Coleoptera: Scolytidae). Ecological Monographs 53:27–49.

781 Raffa, K. F., and A. A. Berryman. 1987. Interacting selective pressures in conifer-bark beetle systems: A

782 basis for reciprocal adaptations? The American Naturalist 129:234–262.

783 Raffa, K. F., J.-C. Grégoire, and B. Staffan Lindgren. 2015. Natural history and ecology of bark beetles.

784 Pages 1–40 *in* Bark Beetles. Elsevier.

785 R Core Team. 2018. R: A language and environment for statistical computing. R Foundation for Statistical

786 Computing, Vienna, Austria.

787 Restaino, C., D. Young, B. Estes, S. Gross, A. Wuenschel, M. Meyer, and H. Safford. 2019. Forest

788 structure and climate mediate drought-induced tree mortality in forests of the Sierra Nevada, USA. Ecological

789 Applications 0:e01902.

790 Robeson, S. M. 2015. Revisiting the recent California drought as an extreme value. Geophysical Research

791 Letters 42:6771–6779.

792 Rouse, W., R. H. Haas, W. Deering, and J. A. Schell. 1973. Monitoring the vernal advancement and

793 retrogradation (green wave effect) of natural vegetation. Type II Report, Goddard Space Flight Center,

794 Greenbelt, MD, USA.

795 Roussel, J.-R. 2019. lidRplugins: Extra functions and algorithms for lidR package.

796 Roussel, J.-R., D. Auty, F. De Boissieu, and A. S. Meador. 2019. lidR: Airborne LiDAR data manipulation

797 and visualization for forestry applications.

798 Safford, H. D., and J. T. Stevens. 2017. Natural range of variation for yellow pine and mixed-conifer forests

in the Sierra Nevada, Southern Cascades, and Modoc and Inyo National Forests, California, USA. Page 241.

dos Santos, A. A., J. Marcato Junior, M. S. Araújo, D. R. Di Martini, E. C. Tetila, H. L. Siqueira, C. Aoki, A. Eltner, E. T. Matsubara, H. Pistori, R. Q. Feitosa, V. Liesenberg, and W. N. Gonçalves. 2019. Assessment of CNN-Based Methods for Individual Tree Detection on Images Captured by RGB Cameras Attached to UAVs. Sensors (Basel, Switzerland) 19.

Seidl, R., J. Müller, T. Hothorn, C. Bässler, M. Heurich, and M. Kautz. 2016. Small beetle, large-scale drivers: How regional and landscape factors affect outbreaks of the European spruce bark beetle. The Journal of Applied Ecology 53:530–540.

Senf, C., E. M. Campbell, D. Pflugmacher, M. A. Wulder, and P. Hostert. 2017. A multi-scale analysis of western spruce budworm outbreak dynamics. Landscape Ecology 32:501–514.

Seybold, S. J., B. J. Bentz, C. J. Fettig, J. E. Lundquist, R. A. Progar, and N. E. Gillette. 2018. Management of western North American bark beetles with semiochemicals. Annual Review of Entomology 63:407–432.

Shepherd, W. P., D. P. W. Huber, S. J. Seybold, and C. J. Fettig. 2007. Antennal responses of the western pine beetle, *Dendroctonus brevicomis* (Coleoptera: Curculionidae), to stem volatiles of its primary host, *Pinus ponderosa*, and nine sympatric nonhost angiosperms and conifers. Chemoecology 17:209–221.

Shiklomanov, A. N., B. A. Bradley, K. M. Dahlin, A. M. Fox, C. M. Gough, F. M. Hoffman, E. M. Middleton, S. P. Serbin, L. Smallman, and W. K. Smith. 2019. Enhancing global change experiments through integration of remote-sensing techniques. Frontiers in Ecology and the Environment 0.

Shin, P., T. Sankey, M. Moore, and A. Thode. 2018. Evaluating unmanned aerial vehicle images for estimating forest canopy fuels in a ponderosa pine stand. Remote Sensing 10:1266.

Stephenson, N. 1998. Actual evapotranspiration and deficit: Biologically meaningful correlates of vegetation distribution across spatial scales. Journal of Biogeography 25:855–870.

Stephenson, N. L., A. J. Das, N. J. Ampersee, and B. M. Bulaon. 2019. Which trees die during drought? The key role of insect host-tree selection. Journal of Ecology 75:2383–2401.

Stovall, A. E. L., H. Shugart, and X. Yang. 2019. Tree height explains mortality risk during an intense drought. Nature Communications 10:1–6.

Thistle, H. W., H. Peterson, G. Allwine, B. Lamb, T. Strand, E. H. Holsten, and P. J. Shea. 2004. Surrogate pheromone plumes in three forest trunk spaces: Composite statistics and case studies. Forest Science 50.

USDAFS. 2017, December 12. Press Release: Record 129 million dead trees in California. https://www.fs.

828 usda.gov/Internet/FSE_DOCUMENTS/fseprd566303.pdf.

829 USDAFS. 2019, February 11. Press Release: Survey finds 18 million trees died in California in 2018.
830 https://www.fs.usda.gov/Internet/FSE_DOCUMENTS/FSEPRD609321.pdf.

831 Vega, C., A. Hamrouni, S. El Mokhtari, J. Morel, J. Bock, J. P. Renaud, M. Bouvier, and S. Durrieu. 2014.
832 PTrees: A point-based approach to forest tree extraction from LiDAR data. International Journal of Applied
833 Earth Observation and Geoinformation 33:98–108.

834 Vose, J. M., D. L. Peterson, G. M. Domke, C. J. Fettig, L. Joyce, R. E. Keane, C. H. Luce, J. P. Prestemon,
835 L. E. Band, J. S. Clark, N. E. Cooley, A. D'Amato, and J. E. Halofsky. 2018. Forests. In Impacts, Risks,
836 and Adaptation in the United States: The Fourth National Climate Assessment, Volume II [Reidmiller, D.
837 R., C. W. Avery, D. R. Easterling, K. E. Kunkel, K. L. M. Lewis, T. K. Maycock, and B. C. Stewart (eds.)].
838 Pages 232–267. U.S. Global Change Research Program.

839 Wallin, K. F., and K. F. Raffa. 2004. Feedback between individual host selection behavior and population
840 dynamics in an eruptive herbivore. Ecological Monographs 74:101–116.

841 Waring, R. H., and G. B. Pitman. 1985. Modifying lodgepole pine stands to change susceptibility to mountain
842 pine beetle attack. Ecology 66:889–897.

843 Weinstein, B. G., S. Marconi, S. Bohlman, A. Zare, and E. White. 2019. Individual tree-crown detection in
844 RGB imagery using semi-supervised deep learning neural networks. Remote Sensing 11:1309.

845 Wyngaard, J., L. Barbieri, A. Thomer, J. Adams, D. Sullivan, C. Crosby, C. Parr, J. Klump, S. Raj Shrestha,
846 and T. Bell. 2019. Emergent challenges for science sUAS data management: Fairness through community
847 engagement and best practices development. Remote Sensing 11:1797.

848 Young, D. J. N., J. T. Stevens, J. M. Earles, J. Moore, A. Ellis, A. L. Jirka, and A. M. Latimer. 2017.
849 Long-term climate and competition explain forest mortality patterns under extreme drought. Ecology Letters
850 20:78–86.

851 Zhang, W., J. Qi, P. Wan, H. Wang, D. Xie, X. Wang, and G. Yan. 2016. An easy-to-use airborne LiDAR
852 data filtering method based on cloth simulation. Remote Sensing 8:501.